JMEPEG (2013) 22:936–942
DOI: 10.1007/s11665-012-0354-5

1059-9495/$19.00

Simulation of the Evolution of Floor Covering Ceramic Tiles During the Firing

Guillermo Peris-Fajarnés, Beatriz Defez, Ricardo Serrano, and Oscar E. Ruiz

(Submitted March 21, 2010; in revised form July 23, 2012; published online September 19, 2012)

Finding the geometry and properties of a ceramic tile after its firing using simulations, is relevant because several defects can occur and the tile can be rejected if the conditions of the firing are inadequate for the geometry and materials of the tile. Previous works present limitations because they do not use a model characteristic of ceramics at high temperatures and they oversimplify the simulations. As a response to such shortcomings, this article presents a simulation with a three-dimensional Norton's model, which is characteristic of ceramics at high temperatures. The results of our simulated experiments show advantages with respect to the identification of the mechanisms that contribute to the final shape of the body. Our work is able to divide the history of temperatures in stages where the evolution of the thermal, elastic, and creep deformations is simplified and meaningful. That is achieved because our work found that curvature is the most descriptive parameter of the simulation. Future work is to be realized in the creation of a model that takes into account that the shrinkage is dependent on the history of temperatures.

Keywords failure analysis, heat treating, modeling processes

1. Introduction

Several assumptions have to be made to model at some extent the sintering of pure ceramic materials. Some of these assumptions are: (i) no chemical reactions occur, (ii) the particles that compose the material are of the same compound, and (iii) the sintering mechanisms are well defined. Because of the complexity of the materials often used to make floor and wall covering ceramic tiles, these basic assumptions do not hold. However, there is a need for computational models that can predict at least some final properties.

Computational models of the firing can have uses in the prediction of the dimensional parameters of the tile. The acceptable parameters, including curvature, are described in the standard ISO10545-2 (Ref 1). Predicting the curvature of the tile in the oven and after it is cooled is important for the ceramic industry, as an appreciable final curvature can cause the product to be rejected. In addition, an appreciable and non-uniform curvature during the firing can cause the decoration to be damaged or have other effects in the final properties of the tile. In our approach the mean curvature of the surface is defined at every point of the surface. The definition of mean curvature and its discretized form can be found in Ref 2.

This article is organized as follows: Section 2 discusses the current state of art in computer simulation of ceramic tile firing. Section 3 describes the methodology used in this article, as a result of the conclusions of our literature review. Section 4 presents the results of the proposed methodology. Section 5 concludes the article.

Guillermo Peris-Fajarnés and **Beatriz Defez**, Centro de Investigación en Tecnologías Gráficas, Universidad Politécnica de Valencia, Valencia, Spain; and **Ricardo Serrano** and **Oscar E. Ruiz**, CAD CAM CAE Laboratory, Universidad EAFIT, Medellín, Colombia Contact e-mails: gperis@upv.es, bdefez@degi.upv.es, rserrano@eafit.edu.co, and oruiz @eafit.edu.co.

2. Literature Review

The "fit-to-reality" approach when modeling the sintering of a ceramic solid uses full constitutive equations. Full constitutive equations include parameters obtained from the microscopic structure of the powder to calculate the shape of the body. Full constitutive equations need parameters that are complex to obtain and define. Simulations and equations do change with the stages of the sintering, so they should then be defined and considered on a specific time and context. This approach is used in Ref 3-5. Even for the purest ceramics,

Nomenclature

$H(S,p)$	Mean curvature of a surface S at a point p
H_{upp}	Set of discrete mean curvatures at the nodes of the upper face of the ceramic tile
H_{low}	Set of discrete mean curvatures at the nodes of the lower face of the ceramic tile
ε_{th}	Set of thermal strains in one direction. Von Misses thermal strains are not defined
$V\varepsilon_{el}$	Set of Von Mises elastic strains
$V\varepsilon_{cr}$	Set of Von Mises creep strains
$V\sigma$	Set of Von Mises stresses
$\overline{M}$	Average of set M. The set can be: $H_{low}, H_{upp}, \varepsilon_{th}, V\varepsilon_{cr}, V\varepsilon_{el}$, or $V\sigma$
std.dev.M	Standard deviation of set M
$\max(M)$	Maximum absolute value of set M
$\sigma_1, \sigma_2, \sigma_3$	Set of first principal, second principal, and third principal stresses, respectively

certain stages of the sintering require phenomenological parameters, that is, parameters from experimental models rather than from microstructure models. Mixed models, like the ones used in Ref 6, 7 use phenomenological constitutive equations in stages where the sintering is more complicated and full constitutive equations in stages where the microstructural parameters can be found. Full constitutive equations need parameters that are difficult to obtain and there are many complications in the simulations as the equations change with the stages of the sintering.

Trying to reduce the number of parameters and the difficulty to obtain them, some simulations restrict their objectives. For example, they only use geometric parameters like linear shrinkage to obtain the final shape of the solid. Ref 8 presents a simulation that uses the principle of the Master Sintering Curve (Ref 9), which states that the geometric parameters used in constitutive equations are functions only of density for a given powder and green-body process. The parameters used are fewer, but they have to be obtained for every powder process. This makes the experiments difficult to replicate. As usual, there is a definite shortage of report on traditional ceramics.

In continuum mechanics, constitutive equations that do not rely in the microstructure of the material are used. Macroscopic constitutive equations that do not rely in the microstructure are able to explain the changes of the shape using simple parameters like elastic, thermal, and creep deformations; or mechanical stresses. Calculating mechanical stresses when the body is at low temperatures allows finding the possibility of brittle fracture. In traditional ceramics, the complexity of the materials and processes involved is high. This is the reason why only a macroscopic approach that does not take into account the microstructure of the material can be used. Few simulations of the firing of ceramic tiles have been made. In Ref 10, 11 a linear approach is used to simulate the deformation of a ceramic tile. However, the behavior that stoneware (the most common material used for floor covering ceramic tiles), shows at high temperatures is nonlinear. In Ref 12 a nonlinear constitutive equation is used. However, the model is not characteristic of ceramics at high temperatures and it is used because it fits the data. In this reference, the authors argue that Norton's model was not used because for different forces applied to a specimen, different parameters that fit the model are obtained. The subject has been widely studied and it is known to be a characteristic of ceramics (Ref 13, 14). The model in Ref 12 only considers displacements in two directions, which does not comply with the physical problem. In that reference, strains are averaged through the thickness of the specimen, which over-simplifies the problem.

3. Methodology

Our simulation is divided into two physical problems: (i) a thermal simulation, which calculates the distribution of temperatures in the body, and (ii) a structural simulation, which uses the temperatures to calculate the thermal deformations and the resulting stresses and mechanical strains that the thermal deformations produce. The deformation of the ceramic tile appears because of the difference of temperatures between the lower and upper faces, which causes the body to have different expansions across the depth of the thickness.

The evolution of the different mechanical, thermal, and geometric parameters of a tile with defined thickness is first evaluated. This thickness is representative and allows the observation of the evolution of the parameters of the tile independent of the thickness. After that, tiles with different thicknesses are also evaluated so the evolution of the parameters can be parameterized. Table 1 shows the geometric parameters of the tile.

For the thermal simulation, constant different temperatures were applied at the upper and lower faces of the tile. Table 2 shows these parameters.

The program of temperatures was characteristic of ceramic tiles firing. It can be seen in Fig. 1.

For the structural problem the tile is minimally constrained so equations can be formulated and solved, without restricting deformations in any direction. A linear coefficient of thermal expansion (α) is used. The data was digitized (Ref 15) from Ref 12 and is shown in Fig. 2.

Norton's model is shown in Eq 1.

$$\frac{d\varepsilon(t)}{dt} = \frac{d\sigma(t)}{dt}\frac{1}{\eta} + A\sigma(t)^n \qquad \text{(Eq 1)}$$

In Eq 1, $\varepsilon(t)$ is the strain as a function of time, $\sigma(t)$ is the tensile stress, η is Young's modulus. A and n are temperature-dependent constants that define the creep behavior of Norton's model.

In this paper, parameters for Norton's model that fit the data from Ref 12 have been found. The stress-relaxation data was divided in two: (i) a fast application of the load in which the deformation is assumed as elastic and (ii) a measure of the stress required to maintain the strain obtained after (i). The

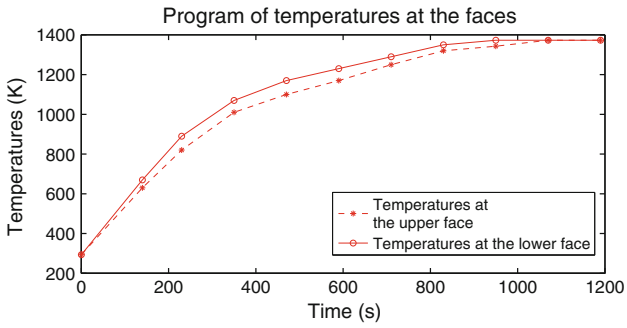

Fig. 1 Temperatures in each of the surfaces of the tile as a function of time in the oven

Table 1 Geometric parameters of the tile

Parameter	Value
Sides of the tile	33 cm × 33 cm
Defined thickness	20 mm
Variable thickness	14, 18, 20, and 24 mm

Table 2 Thermal parameters of the tile

Parameter	Value
Density of the tile (ρ)	2150 kg/m^3
Thermal conductivity (k)	0.57 W/(m K)
Heat capacity (c)	1250 J/(kg K)

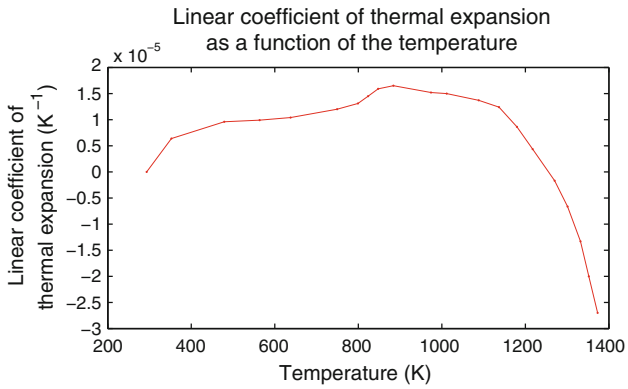

Fig. 2 Linear coefficient of thermal expansion as a function of the time

Table 3 Structural constants of the constitutive model for the study

T, K	η, GPa	A, s^{-1}	*n*
293.15	3.06	0	…
773.15	3.75	2.289×10^{-26}	5
973.15	4.48	4.010×10^{-28}	5
1073.15	4.63	1.164×10^{-27}	5
1173.15	6.07	1.778×10^{-21}	4.27
1173.15	6.63	5.046×10^{-8}	2.42
1273.15	6.49	1.418×10^{-6}	2.30
1323.15	3.14	7.358×10^{-7}	2.44

graphs were digitized and the parameters η, A, and n were obtained. Non-linear least squares regression was used to fit the parameters (Ref 16, 17). Table 3 shows the parameters obtained.

Our simulation used ANSYS® for the FEA (Ref 18). We selected the elements SOLID90 for the thermal problem and SOLID186 for the structural problem. Our simulations include large deformations. The total time spent by each simulation was around 30 days using two Core 2 Duo Processors at 2.33 GHz and 1.7 GB of RAM.

The curvatures as a function of the time have been evaluated using the algorithm from Ref 2. The average was calculated as $\sum H/n$, where n is the number of nodes. H at the borders has been interpolated from the value at the neighbor nodes interior to the face.

4. Results

4.1 Evolution of the Tile with Defined Thickness

In Fig. 3 a summary of the curvatures as function of the time is shown.

The structural problem had four important variables: (i) the thermal strains, (ii) the elastic strains, (iii) the creep strains, and (iv) the stresses. Von Mises elastic and creep strains summarize mechanical strains as Von Mises stresses summarize stresses. The creep formulations in ANSYS® depend on the Von Mises stresses. Since the thermal strains are equal in all directions, the Von Misses formulation cannot be applied. As an alternative,

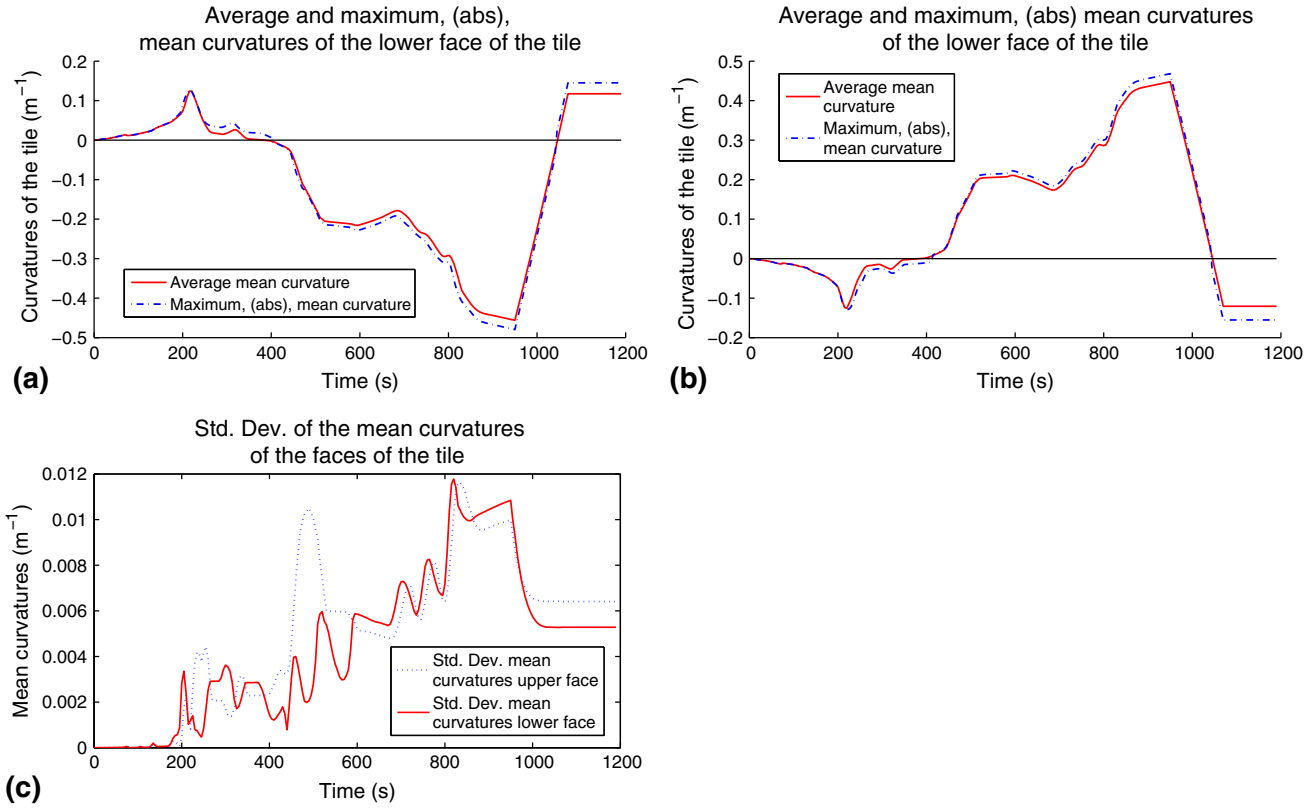

Fig. 3 (a) $\overline{H_{low}}$ and max(H_{low}), (b) $\overline{H_{upp}}$ and max(H_{upp}), and (c) std.dev.H_{low} and std.dev.H_{upp}, as functions of the time

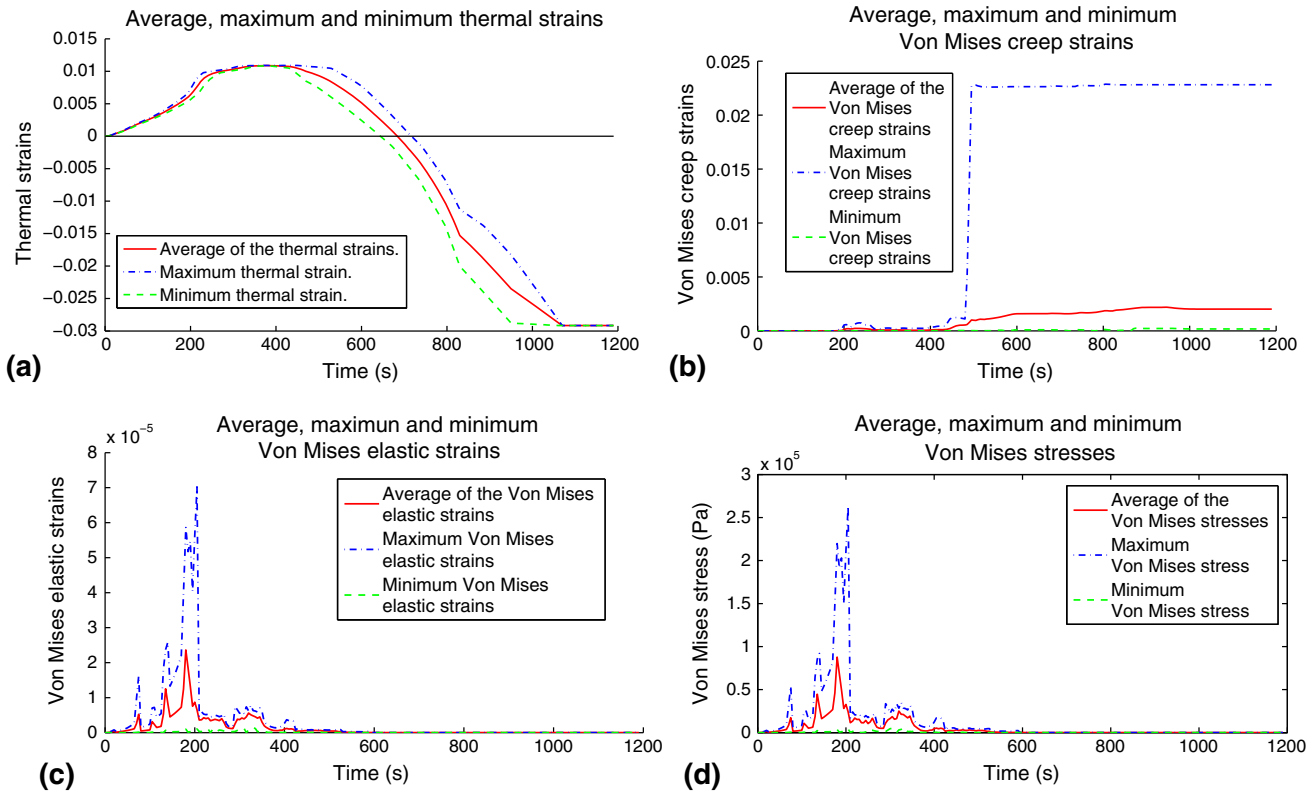

Fig. 4 The evolution of strains and stresses is shown. (a) ε_{th}, (b) $V\varepsilon_{cr}$, (c) $V\varepsilon_{el}$, and (d) $V\sigma$

the value of the thermal strains in one direction was used to summarize them instead. Figure 4 shows average, maximum, and minimum stresses and strains for the tile with thickness 20 mm during the time in the oven.

According to the curvature, the firing of the tile can be divided in three stages.

4.1.1 First Stage. As the ceramic body starts to expand, the lower face becomes convex and the upper face turns concave. The stage continues until the absolute values of $\overline{H_{low}}$ and $\overline{H_{upp}}$ reach a maximum. The maximum temperature at the end of the stage is near the temperature of the maximum thermal expansion coefficient (884 K, Fig. 2). This stage corresponds to the time interval [0 s, 218 s]. Elasticity is the main phenomena; the highest peaks of stresses appear and the possibility of failure because of brittle fracture is higher. The maximum stress reached in the program of temperatures was 0.263 MPa, at 205 s. As a comparison, the mechanical strength of a ceramic tile after drying has been measured as 2.20 MPa (Ref 19).

4.1.2 Second Stage. It corresponds to the time interval [218 s, 950 s]. The second stage is the most important for the final properties of the tile. $\overline{V\varepsilon_{cr}}$ becomes much higher than $\overline{V\varepsilon_{el}}$ and the creep strains, $(V\varepsilon_{cr})$, accumulate to contribute to the final shape of the body. In this stage, $\overline{H_{low}}$ and $\overline{H_{upp}}$ change of sign and reach a maximum absolute value.

The second stage starts when $\overline{H_{low}}$ begins to decrease and $\overline{H_{upp}}$ begins to increase. $\overline{H_{low}}$ and $\overline{H_{upp}}$ become almost 0 at the same time, at 383 s. $\overline{H_{low}}$ keeps decreasing until it reaches a minimum, which coincides with the time at which the lower face reaches the maximum temperature of the program (950 s). Figure 5 shows the distribution of the curvatures at 950 s. Std.dev.H_{low} and std.dev.H_{upp} are high at 950 s and it can be seen that there are many local maxima and minima near the borders. The non-uniformity is a consequence of the high differences among the values of $V\varepsilon_{cr}$ between the center and borders.

In the second stage stresses are relaxed quickly and deformations become more measurable. At the beginning of the stage (218 s), $\overline{V\varepsilon_{cr}}$ in the upper face is higher than in the lower face. This is reversed as the curvature changes of sign. At the end of the stage (950 s), $\overline{V\varepsilon_{cr}}$ is higher in the lower face.

The stresses that produce the creep strains are reactions to the difference of expansions caused by the geometrical gradient of temperatures. Figure 6 displays the first principal stresses, (σ_1), and the third principal stresses, (σ_3). The lower face shows positive values for σ_1 while the upper face shows negative values for σ_3. The lower face is mostly in tension and the upper face mostly in compression, so creep strains should expand the lower face more than the upper, even when the lower face is concave and the upper one is convex, which would seem counter-intuitive. All the second stage has the characteristic that σ_1 is higher in the lower face than in the upper one. The distribution of stresses during the second stage, and the consequent creep strain determine the geometry at the end of the third stage.

4.1.3 Third Stage. It occurs as the differences in the temperature of the body are eliminated. The lower face reaches the maximum temperature at the beginning of the third stage at 950 s. $\overline{H_{low}}$ increases and $\overline{H_{upp}}$ decreases until the temperature of the upper face also reaches the maximum at 1070 s. The change of $\overline{H_{low}}$ and $\overline{H_{upp}}$ between 950 and 1070 s is linear. When the temperature becomes uniform and the residual stresses start to relax, $\overline{H_{low}}$ is positive and $\overline{H_{upp}}$ is negative. At the end of the program, $\overline{V\sigma}$ and $\overline{V\varepsilon_{el}}$ are low. $\overline{H_{low}}$ at the end of the third stage is higher than $\overline{H_{low}}$ at the end of the first stage (which is a local maximum and the maximum of the first stage).

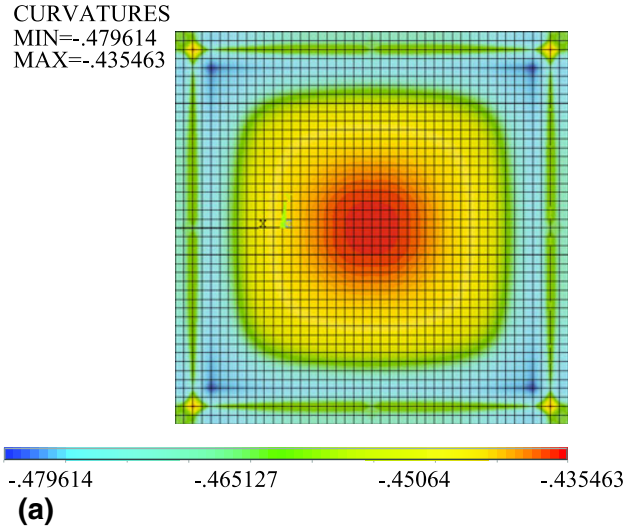

Fig. 5 The distribution of H_{low} and H_{upp} at 950 s

4.2 Comparison of the Evolution of Ceramic Tiles with Variable Thickness During the Firing

The stages that appeared in the 20-mm ceramic tile also appeared in the rest of the geometries. This means that the stages of the mean curvature are only dependent on the program of temperatures and the properties of the tile. They do not depend on the thickness.

Figure 7 displays the evolution of mean curvature and its standard deviation for 4 thickness levels. Figure 7(a) and (b) show the evolution of mean curvatures in the lower and upper face, respectively. Figure 7(c) and (d) illustrate the evolution of the standard deviation of the mean curvature, for the analog cases. Figure 8 shows the average creep strains (Fig. 8a), elastic strains (Fig. 8b), and stresses (Fig. 8c) for the four geometries.

The absolute $\overline{H_{low}}$ and $\overline{H_{upp}}$ increase as the tile thickness decreases. The shapes of the curves were similar, with steeper slopes in the thinner models. Std.dev.H_{low} and std.dev.H_{upp} are higher for the thinnest tiles. However, the shapes of the curves are different, and the curves show a more sensitive behavior to the reduction of thickness than $\overline{H}$.

The maximum $V\sigma$ are the following: (i) thickness 14 mm, 0.474 MPa at 205 s, (ii) thickness 18 mm, 0.314 MPa at 205 s, (iii) thickness 20 mm, 0.263 MPa at 205 s, and (iv) thickness 24 mm, 0.197 MPa at 201 s.

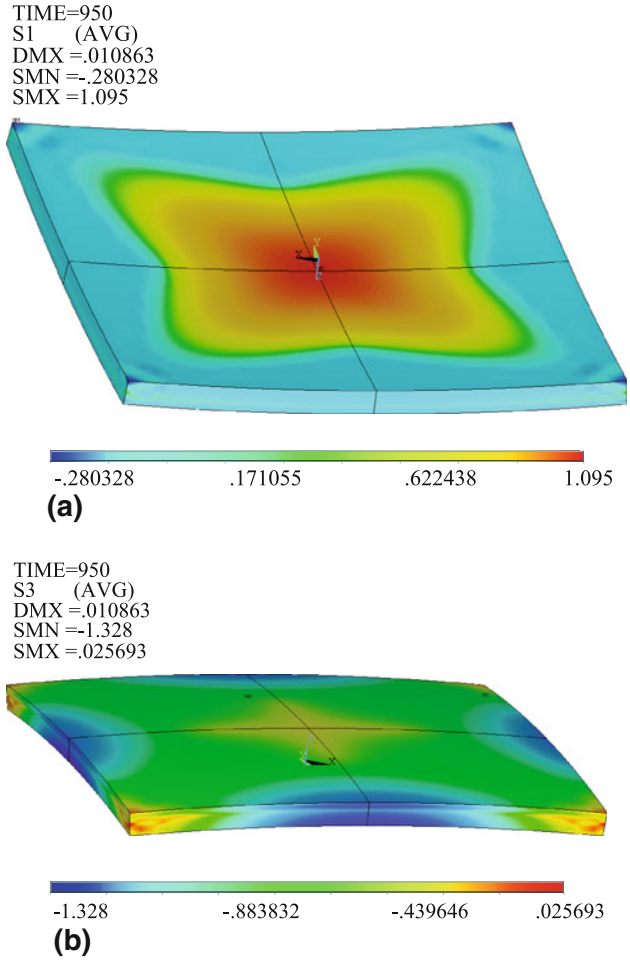

Fig. 6 Distribution of the first and third principal stresses at 950 s

5. Discussion and Conclusions

A flat tile is a goal of the firing itself. The evaluation of the curvature at every point of the tile allows the manufacturer to control more appropriately the temperature in stages where the nonuniformity of the curvature is more notorious. This paper shows that the curvature also helps to divide the firing into stages of the history of temperatures. These stages help to isolate the different effects of the viscoelastic constitutive equation and the thermal expansion of the body. The curvature changes in a more predictable way than the rest of the physical parameters evaluated. The main conclusion of the simulated tests is that the curvature is the most determinant parameter of the history of temperatures and the most important parameter to control when designing a program of temperatures. Other conclusions of the paper are:

(1) The magnitudes of $\overline{H_{low}}$ and $\overline{H_{upp}}$ decrease as the thickness increases, but the local maxima appear at the same time. The shape of the curve of std.dev.H_{low} and std.dev.H_{upp} is not the same for all the thicknesses, but the values are higher with thinner tiles. Std.dev.H_{low} and std.dev.H_{upp} are reflected in

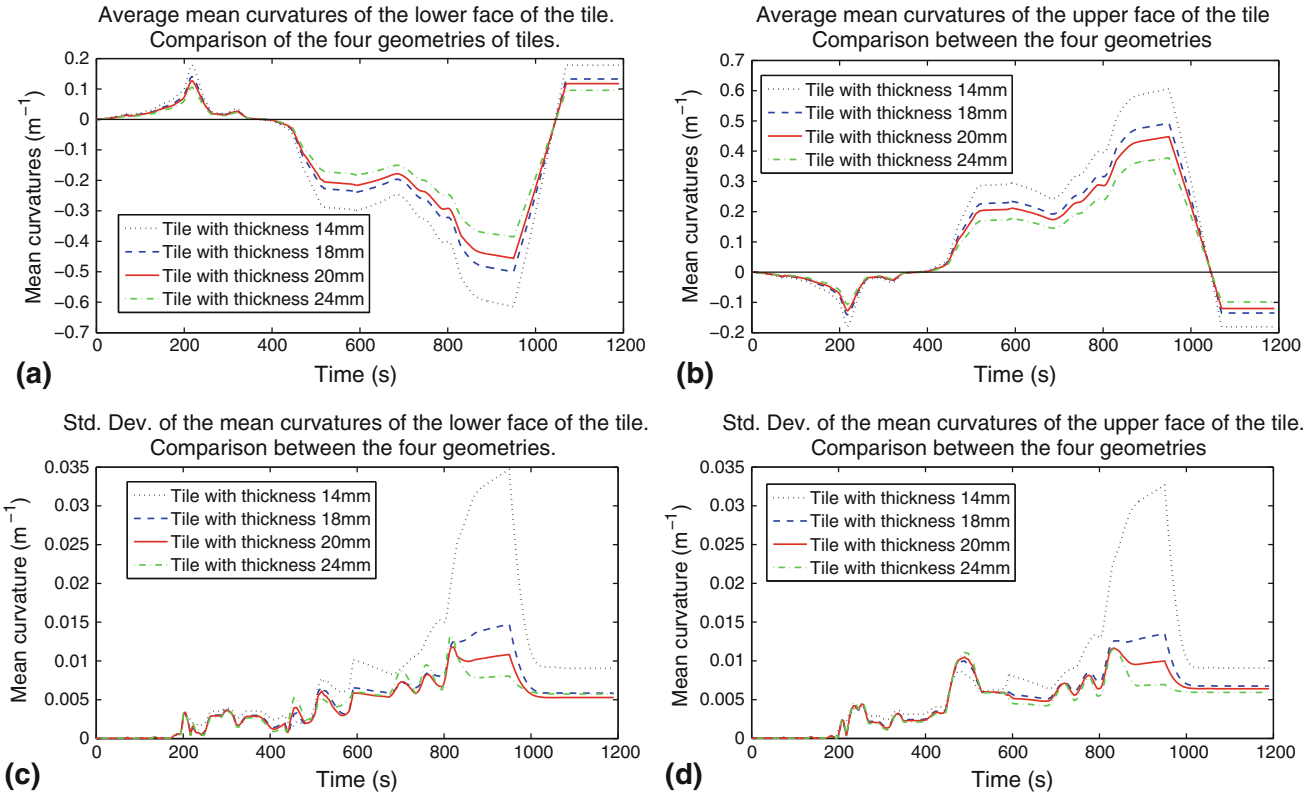

Fig. 7 (a) $\overline{H_{\text{low}}}$ and (b) $\overline{H_{\text{upp}}}$ for the four geometries of ceramic tiles. (c) Std.dev.H_{low} and (d) std.dev.H_{upp} for both faces for the four geometries of ceramic tiles

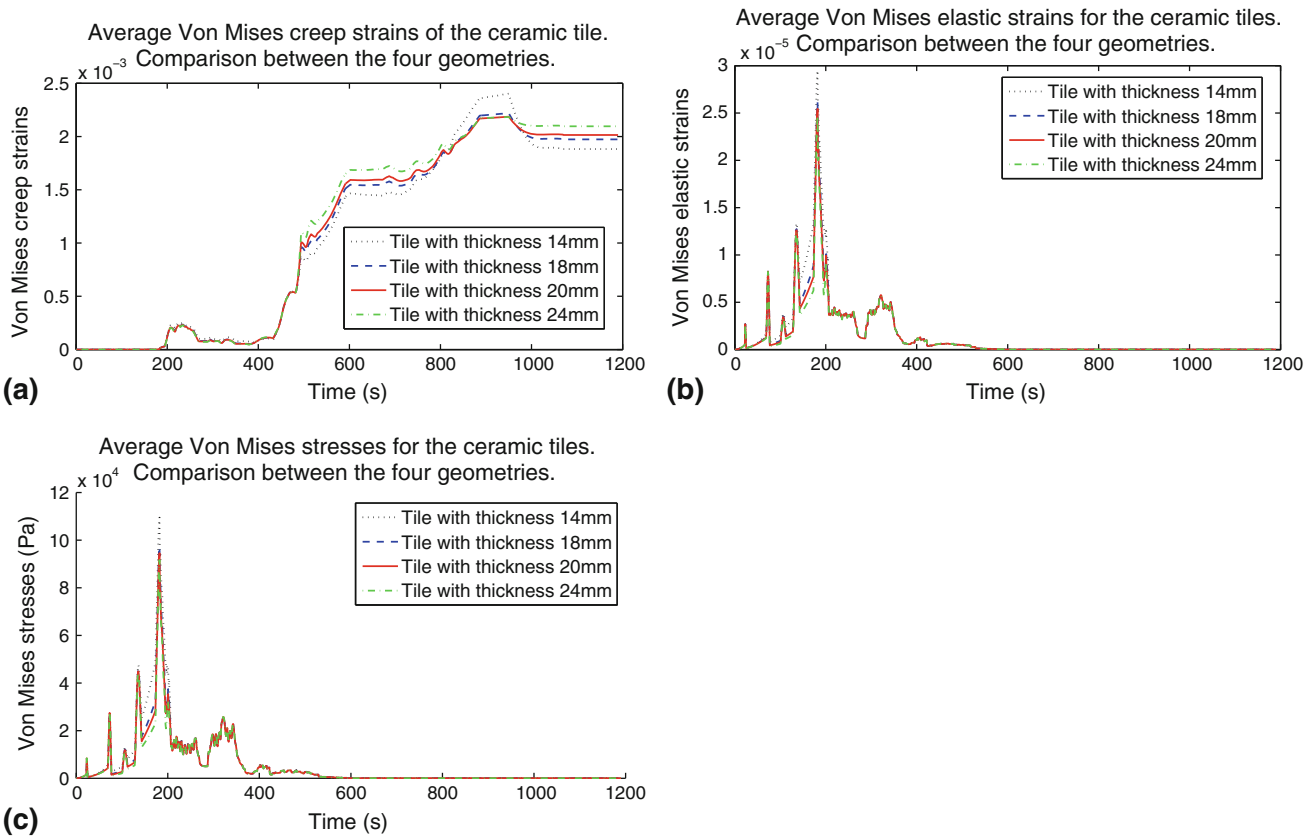

Fig. 8 $\overline{V\varepsilon_{\text{el}}}$, $\overline{V\varepsilon_{\text{cr}}}$, and $\overline{V\sigma}$ of the four geometries of tiles as a function of the time

the homogeneity of the surfaces. The distribution of curvatures indicates that the measurements at different points of the tile are necessary to control the shape of the tile.

(2) The tile at low temperatures has a brittle behavior. To evaluate the possibility of brittle fracture, more constants than just mechanical strength are needed and have to be measured at high temperatures. However, the maximum $V\sigma$ reached by the thinnest tile is much lower than the maximum mechanical strength measured on the dry tile (Ref 19). On the other hand, deformations caused by creep are appreciable and the defects caused are more important and cause more concern to the industry.

(3) When the temperature becomes uniform (and no stresses exist), the curvature of the tile is opposite to the sign that the thermal expansion forces on the tile most of the time in the oven.

6. Future Work

Future work is needed in the creation of a model that takes into account that the shrinkage is dependent on the history of temperatures. In this manner, we will be able to simulate the time interval in the oven when the temperature is sharply decreased until the tile is cold and the curvature is final. Intensive experimental work is also needed to corroborate the simulations.

References

1. ISO. 10545-2:1995, "Ceramic Tiles—Part 2: Determination of Dimensions and Surface Quality," International Standard Confirmed, International Organization for Standardization, Geneva, Switzerland, 31 Dec 2005
2. M. Botsch and M. Pauly. Course 23: Geometric Modeling Based on Polygonal Meshes, *ACM SIGGRAPH 2007 Courses*, 2007
3. E.A. Olevsky and V. Tikare, Combined Macro-Meso Scale Modeling of Sintering. Part I: Continuum Approach, *Recent Developments in Computer Modeling of Powder Metallurgy Processes*, A. Zavaliangos and A. Laptev, Ed., IOS Press, Amsterdam, The Netherlands, 2001, p 85
4. V. Tikare, E.A. Olevsky, and M.V. Braginsky, Combined Macro-Meso Scale Modeling of Sintering. Part II, Mesoscale Simulations, *Recent Developments in Computer Modeling of Powder Metallurgy Processes*, A. Zavaliangos and A. Laptev, Ed., IOS Press, Amsterdam, The Netherlands, 2001, p 94
5. K. Shinagawa, Finite Element Simulation of Sintering Process: Microscopic Modelling of Powder Compacts and Constitutive Equation for Sintering, *JSME Int J., Ser. A*, 1996, **39**(4), p 565–572
6. H. Riedel and T. Kraft, Numerical Simulation of Solid State Sintering: Model and Application, *J. Eur. Ceram. Soc.*, 2004, **24**, p 345–361
7. H. Riedel and B. Blug, A Comprehensive Model for Solid State Sintering and Its Application to Silicon Carbide, *Solid Mech. Appl.*, 2001, **84**, p 49–70
8. J.A. Yeomans, M. Barriere, P. Blanchart, S. Kiani, and J. Pan, Finite Element Analysis of Sintering Deformation Using Densification Data Instead of a Constitutive Law, *J. Eur. Ceram. Soc.*, 2007, **27**, p 2377–2383
9. H. Su and D.L. Johnsonn, Master Sintering Curve: A Practical Approach to Sintering, *J. Am. Ceram. Soc.*, 1996, **79**(12), p 3211–3217
10. H. Camacho, M.E. Fuentes, L. Fuentes, A. Garcia, and A. Perez, Stress Distribution Evolution in a Ceramic Body During Firing. Part 1. Problem Statement, *Bol. Soc. Esp. Ceram.*, 2003, **42**, p 283–288
11. H. Camacho, M.E. Fuentes, L. Fuentes, A. Garcia, and A. Perez, Stress Distribution Evolution in a Ceramic Body During Firing. Part 2. Profile Calculation, *Bol. Soc. Esp. Ceram.*, 2003, **42**, p 353–359
12. V. Cantavella Soler, et al., "Simulación de la deformación de baldosas cerámicas durante la cocción," PhD thesis, 1998
13. W.R. Cannon and T.G. Langdon, Review: Creep of Ceramics. Part 1: Mechanical Characteristics, *J. Mater. Sci.*, 1983, **18**(1), p 1–50
14. W.R. Cannon and T.G. Langdon, Review: Creep of Ceramics. Part 2: An Examination of Flow Mechanisms, *J. Mater. Sci.*, 1988, **23**, p 1–20
15. M. Mitchell. *Engauge Digitizer*, 2009
16. R Development Core Team, *R: A Language and Environment for Statistical Computing*, R Foundation for Statistical Computing, Vienna, Austria, 2009, ISBN 3-900051-07-0
17. G. Grothendieck, nls2: Non-linear Regression with Brute Force, R package version 0.1-2, 2007
18. J. Swanson, Ansys 11.0, Ansys, 2008
19. J.L. Amoros, E. Sanchez, V. Cantavella, and J.C. Jarque, Evolution of the Mechanical Strength of Industrially Dried Ceramic Tiles During Storage, *J. Eur. Ceram. Soc.*, 2003, **23**(11), p 1839–1845